

DESIGN AND MEASUREMENTS OF AN X-BAND ACCELERATING CAVITY FOR SPARC

D. Alesini, M. Ferrario, B. Spataro, INFN/LNF, Frascati (Rome), Italy

A. Bacci, INFN/LASA, Segrate (Milan), Italy

A. Falone, M. Migliorati, A. Mostacci, F. Palpini, L. Palumbo, Univ. "La Sapienza", Rome, Italy

Abstract

The paper presents the design of an X-band accelerating section for linearizing the longitudinal phase space in the Frascati Linac Coherent Light Source (SPARC). The structure, operating on the π standing wave mode, is a 9 cells structure fed by a central coupler and it has been designed to obtain a 42 MV/m accelerating gradient. The 2D profile has been determined using the electromagnetic codes Superfish and Oscar-2D while the coupler has been designed using HFSS. Bead-pull measurements made on a copper prototype have been done and the results are illustrated and compared with the numerical ones. Mechanical details of the realized prototype and RF properties of the structure as a function of the assembly characteristics are also discussed.

INTRODUCTION

The use of an X-Band structure operating at 11.424 GHz is required to compensate the non-linearity distortions due to the RF curvature during acceleration and compression[1] of the SPARC Phase II[2]. The schematic layout is reported in Fig. 1. The X-Band structure, designed to obtain 42 MV/m accelerating gradient, is a 9 cells π -mode structure fed by a central coupler. The fourth harmonic of 2.856 GHz has been chosen for space availability reasons and also because the technologies in the X-Band power sources and modulators have been already developed for future linear collider projects.

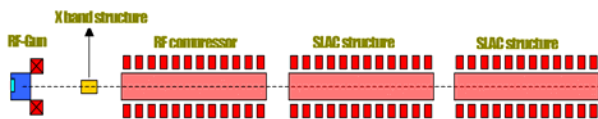


Figure 1: schematic layout of SPARC phase II.

THE X BAND STRUCTURE DESIGN

2D Profile

The detailed analysis of the structure design without coupler is reported in [3]. The 2D structure dimensions are reported in Fig. 2 and have been determined with the 2D electromagnetic (e.m.) codes Superfish [4] and Oscar-2D[5]. The choice of 9 cells has been done to achieve a total accelerating voltage $V=5$ MV with 3 MW of peak input power. No dedicated dampers of the parasitic higher order modes have been adopted since the X-Band structure operates on single bunch. Other cavity parameters are reported in Table 1.

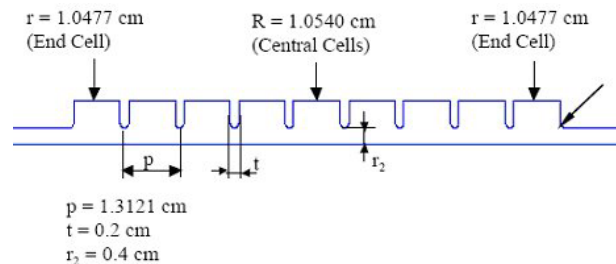


Figure 2: 2D profile of the X-band structure.

Table 1: X-band cavity parameters

Quality factor Q	8400
R/Q [Ω/m]	9165
Average dissipated Power [W]	270
Peak axial E-field [MV/m]	57.5
Kilpatrick factor	1.197
Peak surface electric field [MV/m]	105

Coupler Design

Concerning the coupler design, it has been decided to feed the cavity in the central cell in order not to excite the mode $8/9\pi$ that has the frequency nearest to the π mode and zero field in the central cell. Therefore with a central coupler we have a much greater separation of the modes and, consequently, the working mode is less perturbed by the closest one. To reduce the coupler window dimensions we have decided to taper the smaller dimension of the standard X-band waveguide (10.16 mm) to the dimension of 4 mm. The coupling cell is sketched in Fig. 3.

The dimension of the coupler window (w) and of the central cell radius (R_c) have been tuned in order to obtain simultaneously a coupling coefficient $\beta = 1$, a resonant frequency of the whole system (cells+coupler) equal to 11.424 GHz and to preserve a good field flatness. This has been done using the e.m. code HFSS [6] by following two steps:

a) we have simulated a single cell with coupler and the dimensions of the coupler window and cell radius have been tuned in order to obtain a coupling coefficient $\beta = 9$ (exactly 9 times the coupling coefficient that we would reach with the complete structure) and a cell resonant frequency equal to 11.424 GHz;

b) we have simulated the complete structure with the dimensions found in the previous case and we have slightly adjusted the dimensions of the coupler cell and

window to obtain a perfect field flatness at the resonant frequency of 11.424 with $\beta = 1$.

After this procedure we have obtained the external quality factor $Q_{EXT}=7900$ and the coupling coefficient $\beta = 1.09$ with a good field flatness (within few percent).

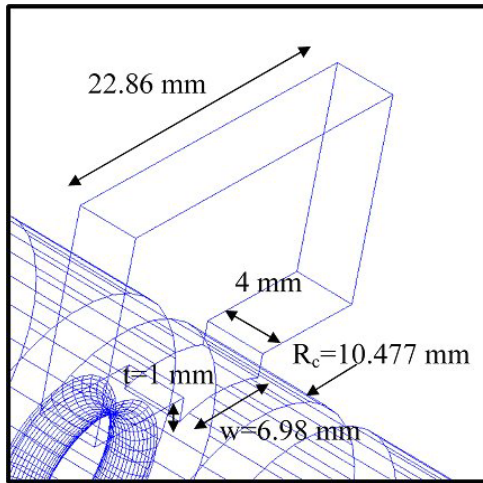


Figure 3: sketch of the coupling cell.

COPPER PROTOTYPE AND MEASUREMENT SETUP

A full scale copper prototype has been constructed and it is shown in Fig 4. The 9 cell structure has been designed for brazing, but the RF tests refer to a mechanically joined structure. The structure has been realised by mechanical machining with a numerically controlled lathe and the obtained precision is below 0.01 mm, while the surface roughness is not worse than $0.4 \mu R_a$. The surface finishing was obtained directly by mechanical machining with custom cutting tools, avoiding any polishing technique and only silicon and sulphur free cutting fluid was used. Each cell dimension has been checked with a quality control test. The final machining was done at constant temperature in order to guarantee as much as possible the uniformity of the mechanical dimensions of the cells.

The assembling procedure foresees the joining of the nine cells using two stainless steel disks used to press the structure by means of three 8 mm diameter copper rods. A torque of 5 Nm corresponds to a pressure of roughly 80 N/mm².

Two type of different measurements have been done:

- a) transmission (or reflection) scattering coefficients measurement between the two lateral antennas or between the antennas and the central coupler;
- b) bead pull measurements.

With the first type of measurements we have found the resonant frequency, the β coefficients of the input ports and the unloaded or external quality factors of π (or other) mode(s). With the second type of measurements we have found the longitudinal electric field on axis and we have calculated the shunt impedance of the structure.



Figure 4: copper prototype of the X band structure.

MEASUREMENTS RESULTS

The transmission coefficient between the two small antennas and between the antenna and the central coupler are reported in Figs. 5a and 5b respectively. As previously observed, we can excite only 5 over 9 possible modes by the central coupler because we impose a non-zero field in the central cell. On the contrary with the two antennas we can excite all the possible modes. The quality factor of the resonance has been measured as a function of pressure realized by the rods. The measured quality factors, unloaded and external, agree with the theoretical one within few percent even if the structure is not brazed. As an example the quality factor of the resonance has a function of pressure realized by the rods is reported in Fig 6.

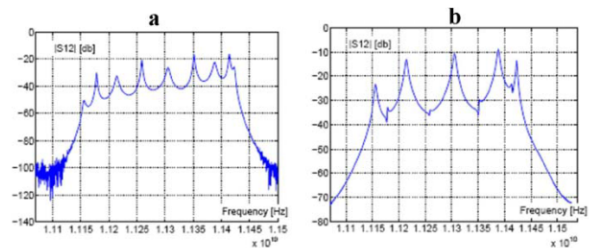


Figure 5: transmission coefficients between the two small antennas and coupler input port.

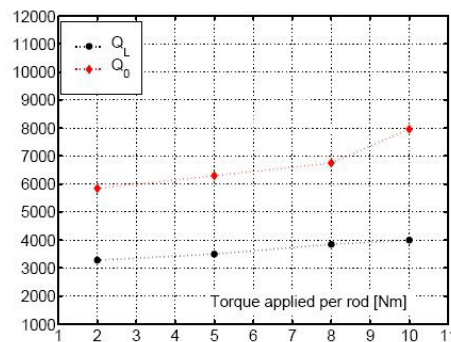


Figure 6: measured quality factor of the π mode resonance as a function of pressure realized by the rods.

The measured dispersion curve, compared with the one obtained from HFSS and SUPERFISH, is reported in Fig. 7.

With the bead pull technique we have measured the electric field on axis. A careful optimization of the measurement setup has been done in order to minimize the systematic errors and to better understand the uncertainty of the measurements. The most important reasons of induced errors in the measurements were:

a) the effect of nylon wire that induced an unwanted perturbation in the frequency measurement. To cancel this systematic error different measurements have been done with different nylon wire diameters. A typical phase resonance measurement with different wire diameters is reported in Fig. 8. The best results have been obtained with the smallest wire and the final small systematic error has been completely cancelled considering the frequency shift with and without the perturbing object;

b) the effect of the drops of glue used to fix the perturbing object. It gave a perturbation in the frequency measurement of the order of 10% of the total frequency variation. To take into account this effect different measurements have been done in order to subtract the systematic perturbation to the measure;

c) the effect of jitter in the longitudinal coordinate between different measurements and within a single measure. This problem, given by the stepping motor, has been reduced using a weight no more than 75 g, and correcting off-line the measurement results.

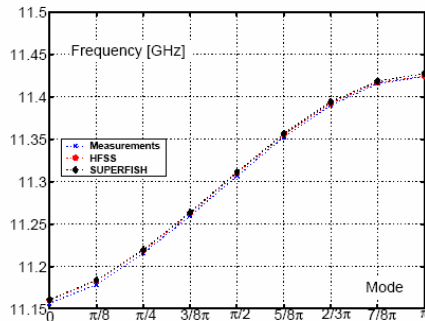


Figure 7: measured dispersion curve.

To calculate the R/Q of the structure it has been necessary to determine the form-factor of the different perturbing objects. Using Slater's theorem we have calibrated the form factor comparing the perturbation induced by the perturbing object in a cavity with known field with the analytical result. For this purpose, It has been used a pill-box cavity working at 1.91 GHz on the TM_{010} mode. Using different resonant mode of the pillbox cavity we have also checked that the form-factor does not depend on the frequency. The measured longitudinal electric field on axis, after the tuning procedure, is plotted in Fig. 8. The reached field-flatness is of the order of 1% at the nominal resonant frequency of 11.424GHz.

The calculated R_{sh}/Q_s normalized to the cavity length is ≈ 9500 and it is in very good agreement with the simulation results.

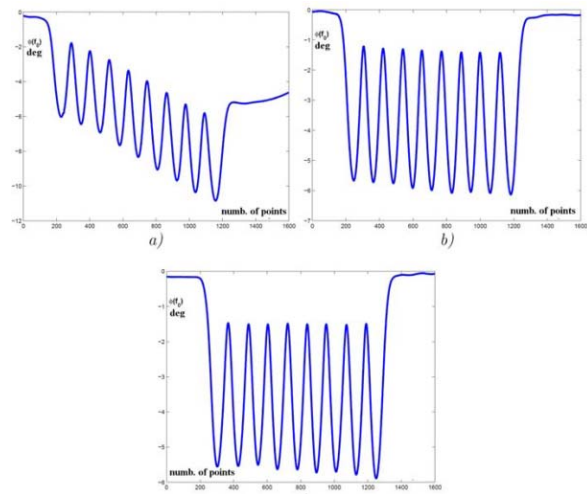


Figure 8: phase of resonance measurement with different wire diameters: a) 0.18 mm; b) 0.148 mm; c) 0.083 mm.

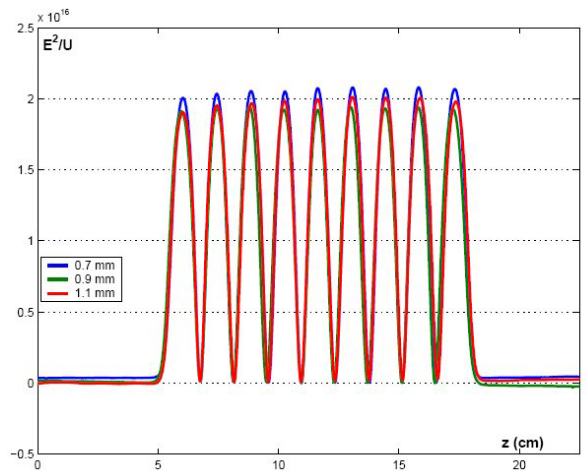


Figure 8: measured longitudinal electric field on axis.

CONCLUSIONS

In the paper we have presented the design of the X-band accelerating section for linearizing the longitudinal phase space in the Frascati Linac Coherent Light Source (SPARC). Quality factors, resonant frequency and electric field measurements have been done on a copper prototype. Even if the prototype is not brazed the reached quality factors are very close to the theoretical ones. Concerning the electric field measurement with the bead pull technique we have discussed the most important reasons of induced errors and how to cancel these effects. Brazing tests are now in progress in the LNF for the construction of the final device.

REFERENCES

- [1] P.Emma, LCLS-TN-01-1, SLAC 2001.
- [2] SPARC Injector TDR, www.lnf.infn.it.
- [3] A. Bacci et al., LNF 03/008(R), Frascati, (2003).
- [4] J. H. Billen and L. M. Young, Part. Acc. 7 (4), 1976.
- [5] P. Fernandes and R. Parodi, PAC 1982.
- [6] www.ansoft.com.